View metadata, citation and similar papers at core.ac.uk

brought to you by CORE

provided by Open Archive Toulouse Archive Ouverte

Open Archive Toulouse Archive Ouverte

OATAO is an open access repository that collects the work of Toulouse researchers and makes it freely available over the web where possible

This is an author's version published in: http://oatao.univ-toulouse.fr/27147

Official URL:

https://doi.org/10.1016/j.ijhydene.2020.03.120

To cite this version:

Carrère, Pierre and Prat, Marc Impact of the anode operating conditions on the liquid water distribution in the cathode gas diffusion layer. (2021) International Journal of Hydrogen Energy, 46 (33). 17534-17549. ISSN 0360-3199.

Any correspondence concerning this service should be sent to the repository administrator: tech-oatao@listes-diff.inp-toulouse.fr

Impact of the anode operating conditions on the liquid water distribution in the cathode gas diffusion layer

Pierre Carrère, Marc Prat[*]

Institut de Mécanique des Fluides de Toulouse (IMFT), Université de Toulouse, CNRS, Toulouse, France

Keywords:
Water management
Pore network modelling
Anode cathode model
PEMFC

ABSTRACT

Previous experimental results indicate that the humidification conditions at the anode have an impact on the liquid water distribution in the cathode gas diffusion layer. Numerical simulations are developed to reproduce and analyze this effect. Results consistent with the experimental results are first obtained by playing with the partition coefficients of an advanced pore network model computing the liquid water formation and transfer in the cathode gas diffusion layer (GDL) for a large range of operating conditions. Then, a model for the full anode cathode assembly is developed by combining the pore network model of the cathode GDL and a 1D model describing the heat and water transfer in the various components of the anode cathode assembly. This enables one to generalize the dry wet regime diagram introduced in a previous work by incorporating the effect of the humidity condition at the anode.

Introduction

In a PEM Fuel Cell, the electrochemical reaction takes place at the cathode Catalyst Layer (CL). This exothermic reaction generates electricity, produces water and releases heat. The water in excess must exit the Fuel Cell (FC). The shortest pathway is to cross the cathode Gas Diffusion Layer (GDL) in order to reach the gas channels of the Bipolar Plate (BP) where the existing gas flow can transport the water out of the fuel cell. Another main role of the cathode GDL is to improve the diffusion of the reactant gas from the gas channels to the entire surface of the cathode CL in order to make the reaction happen everywhere. This gas transport has a direct impact on the efficiency of the PEMFC. In this respect, the presence of liquid water in the GDL has a detrimental effect since the pores of the GDL occupied by liquid water are local barriers for

* *Corresponding author.*
E mail address: mprat@imft.fr (M. Prat).

the reactant gas transport. In other words, the cathode GDL is a key component regarding the PEMFC water management issue and understanding better the factors controlling the occurrence of liquid water in the cathode GDL is a major topic of interest. Not surprisingly, a lot of research has been performed on this topic.

On the experimental side, quite a few works have been dedicated to the observation of liquid water distributions in GDLs in operating FCs using X Ray tomographic microscopy [1–9] or neutron radiography [10–12]. These works have shown the impact of the operating conditions (temperature, current density, relative humidity of the gas at the cathode side) or the impact of the GDL design (felt type GDLs versus paper type GDLs [8], impact of the thickness of the GDL [9], new designs of GDL with patterned wettability [12] or new microstructures [4]).

On the modelling side, several models have been developed or used for studying the formation and transport of liquid water in the cathode GDL. Different numerical techniques have been used [13] such as pore network modelling (PNM) [14–34], the Lattice Boltzmann Method (LBM) [35–37], the volume of fluids (VOF) method [38], the water path network method [39,40] and others. It has recently been shown that due to the anisotropy and the thinness of GDLs, no representative elementary volume could be clearly defined [41] to take into account all the pore scale inhomogeneities. Therefore, it is recommended to prefer approaches at the scale of the pore network rather than volume averaged descriptions, also referred to as macro homogeneous models or continuum models. In this context, pore network models have the advantage to be computationally much faster than direct methods such as the LBM or the VOF method for instance. For these reasons, PNM has become a popular approach for the simulation of the liquid water formation and transport in PEMFC GDLs. The present paper also relies in part on PNM. Regarding pore network modelling, the first works were based on the more or less implicit assumption that the water produced at the cathode CL enters the cathode GDL in liquid phase. This assumption is actually made in the majority of the works based on PNM [14–26]. Since only the transport of water in liquid phase is considered in these models, they are referred to as Liquid Injection Pore Network Models (LIPNM). However, as discussed for instance in Ref. [29], the liquid phase distributions in the GDL predicted by the LIPNM are very often in clear disagreement with the in situ experimental observations. An obvious shortcoming of LIPNM models is that they do not explicitly take into account the operating conditions (current density, temperature, relative humidity in the channel). For this reason, improved PNM models have been developed based on the consideration that i) the produced water might enter the GDL in vapour phase and not in liquid phase and ii) liquid vapour phase change phenomena (evaporation and condensation) are a key aspect [29–34]. As shown in Ref. [29], this led to results quite consistent with experimental observations. This type of PNM is referred to as a Condensation Pore Network Model (CPNM) since the occurrence of liquid water in the GDL pores is only due the condensation of the vapour in a CPNM. However, the liquid water distributions predicted by the CPNM are not fully consistent with some observations, in particular for highly

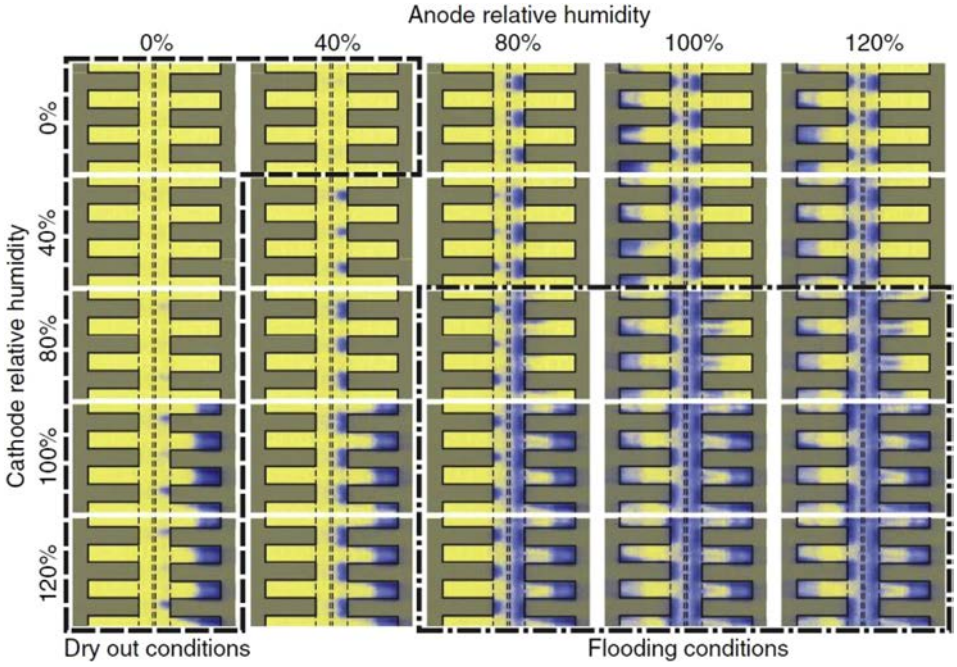

Fig. 1 – Liquid water distributions in operating PEMFC reported in Ref. [10] when varying RH_a and RH_c. The cathode side is on the right hand side of the 2D fuel cell and the anode is on the left hand side. Republished with permission of Electrochemical Society Inc., from [Local Characterization of PEFCs by Differential Cells: SystematicVariations of Current and Asymmetric Relative Humidity, P. Oberholzer & P. Boillat, Journal of the Electrochemical Society, 161 (1), 2014]; permission conveyed through Copyright Clearance Center, Inc.

humidified gas in the cathode bipolar plate channels. For this reason, additional developments in the PNM were made leading to the currently most advanced PNM, referred to as the Mixed Injection Pore Network Model (MIPNM) [30,31]. The latter takes into account both the possible intrusion of the water into the GDL in liquid phase as well as the transport in vapour phase and the condensation evaporation phenomena. As reported in Ref. [30], this model leads to a quite good agreement with experimental observations over a quite large range of operating conditions.

However, the different CPNMs and the more recent MIPNM, take into account the operating conditions at the cathode side only. Experimental observations in Ref. [10] suggest that this is not sufficient and that the conditions at the anode have also an impact. In Ref. [10], liquid water distribution in all the components of the anode cathode assembly (gas channels, GDLs, CLs and membrane) is reported for different operating conditions. In particular, for a given current density i 1 A cm ^{2} and a given temperature T 70 °C the relative humidity at both the anode and cathode sides has been varied. The corresponding liquid water distributions from Ref. [10] are presented in Fig. 1. As can be seen, for a given relative humidity RH_c in the cathode channel gas (this corresponds to a given horizontal row in Fig. 1), the relative humidity RH_a in the anode channel gas has an impact on the liquid water distribution in the cathode GDL. Overall, the higher is RH_a, the higher the water saturation in the cathode GDL. For instance, for RH_c 80%, the cathode GDL remains dry for RH_a 0%. The liquid water appears in the region below the ribs only for RH_a 40% whereas liquid water can be observed in all the regions of the cathode GDL both below the ribs and below the channels for $RH_a \geq 80\%$.

As will be discussed below, this impact of the anode operating conditions can be taken into account with the CPNMs [28–34] or the MIPNM by playing with the fraction of the produced heat and the fraction of the produced water going toward the cathode. However, a more satisfactory approach is to predict these fractions. To this end, a whole anode cathode assembly model is necessary.

Several numerical models have modelled the whole anode cathode assembly [42–46]. However, these are macro homogeneous models based on the continuum approach to porous media. As a result, these models are limited and are not able to predict the details of the 3D liquid water distribution in the cathode GDL which is of great interest regarding the water management issue. Nevertheless, while the pore network approach is preferred for the modelling of the cathode GDL, the continuum approach appears less questionable for the other components. The CL is a porous material but its representation by a pore network implies the generation of very big pore network because of its much finer microstructure compared to the GDL [47–49]. This makes the computational times much larger than for a GDL for a comparatively similar computational domain size. Also, the length scale separation is less an issue than for the GDL. The same holds for the micro porous layer (MPL) [50,51] located between the GDL and CL. The continuum approach is also reasonably well adapted to the membrane, a polymeric material quite different from a porous material. An attractive approach is then to rely on PNM for the GDL and continuum models (CM) for the other components.

However, only a limited number of works have developed a whole anode cathode assembly model able to predict the liquid water distribution in the cathode GDL. In Ref. [52] a Pore Network Model for the GDL is coupled with a continuum approach to model the other components of the assembly. The PNM in Ref. [52] can simulate the vapour transfer, the liquid water transport and the phase change. The model presented in Refs. [52] has not been used to study the impact of the anode operating conditions. However, it can be noted that it was used in Ref. [53] to study the impact of the GDL at the anode on the water management. A full anode cathode assembly model using PNM is also presented in Ref. [32] and in Ref. [54]. However, this model does not really simulate the liquid water formation. It is just assumed that 10% of the GDL pore volume is filled with liquid water. In the present article, the impact of the anode operating conditions on the liquid water distribution in the cathode GDL is studied. The issue is explored by using the MIPNM only in a first step. The MIPNM of the cathode GDL is then coupled with a full anode cathode assembly 1D model in a second step.

The paper is organized as follows. The main features of the MIPNM are first briefly recalled. Then simulations with the MIPNM models for various values of the heat flux and water

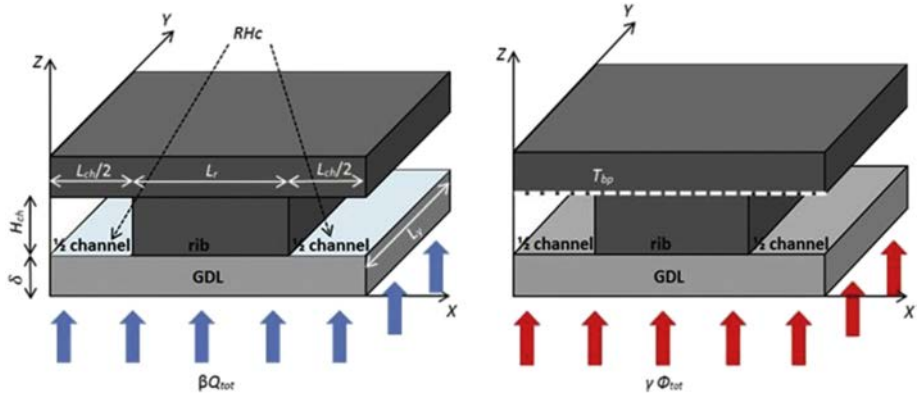

Fig. 2 – Sketch of the GDL unit cell and schematics of water (left) and heat (right) transfer problems. The simulations are performed for L_r L_{ch} 1 mm, δ 0.2 mm and H_{ch} 0.6 mm.

flux partition coefficients are presented. Then, the anode cathode coupled PNM continuum model is presented. Re sults with the coupled model are presented and discussed. The papers ends with the section devoted to the main con clusions of the study.

MIPNM

A summary of the main features of the MIPNM is given in this section. One can refer to Ref. [30] for the details. The MIPNM simulates the water formation and transport in a cathode GDL unit cell. As sketched in Fig. 2, the GDL unit cell corresponds to a subdomain located between the cathode CL/MPL on one side and a central rib surrounded by two half channels on the other side. The GDL unit cell is modelled by generating a 3D cubic pore network. The following phenomena are taken into account: heat transfer, water vapour diffusion, liquid vapour phase change, i.e. condensation and evaporation, capillarity controlled liquid displacement. Note that the MIPNM can predict liquid − phase exhaust at the GDL outlet. The condi tion is a free exit condition in the channels.

The main features of the model can be listed as follows:

- A fraction γ of the total heat flux Φ_{tot} produced in the CL is transferred toward the cathode GDL while the BP temper ature T_{bp} is imposed as sketched in Fig. 2.

$$\Phi \quad \gamma\Phi_{tot} \quad \gamma\left(\frac{h_r}{2F}+U\right)i \tag{1}$$

where h_r is the reaction enthalpy (h_r 242 kJ mol ^{1}), F is the Faraday's constant (F 96485.34C) and U is the voltage.

- The molar flux of water Q entering at the GDL inlet, i.e coming from the CL, is a fraction β of the water flux pro duced by the electrochemical reaction Q_{tot}.

$$Q \quad \beta Q_{tot} \quad \beta\frac{i}{2F} \tag{2}$$

The relative humidity RH_c in the gas flowing in the cathode channel is imposed as sketched in Fig. 2.

- If the computed local relative humidity in an element (pore or throat) is equal or greater than one, condensation happens.
- Depending on the operating conditions, water can be injected at the inlet in both liquid and vapour phases. When there is liquid injection, the liquid injection points are randomly chosen over the GDL inlet. The density of injection points α is a parameter of the model.
- The liquid water displacement is controlled by the capillary effects.

To sum up, the MIPNM inputs are: the BP temperature T_{bp}, the current density i and the relative humidity RH_c of the gas in the cathode channel. The voltage U is also an input of the model determined from a chosen experimental polarization curve. Three parameters permit the calibration of the model: the density of liquid injection points α which mimics the role of the non modelled MPL located between the CL and the GDL, the water partition coefficient β and the heat partition coeffi cient γ.

Table 1 − Experimental operating conditions considered in Ref. [10].

Temperature T_{bp}	70 °C
Current density i	1 A cm ^{2}
Gas pressure P	2 bar
Voltage U	0.54 V *

* The value of the voltage is set to $U = 0.54$ V for all the values of (RH_a, RH_c). $U = 0.54$ V is a mean value. Actually, it has been measured that U varied between 0.46 V for ($RH_a = 0\%$, $RH_c = 0\%$) and 0.62 V for ($RH_a = 100\%$, $RH_c = 0\%$).

Simulation conditions

The simulation conditions are the operating conditions in the experiments presented in Ref. [10]. The corresponding values, set for all the simulations, are recalled in Table 1. In the ex periments [10] the values of RH_a and RH_c were varied imposing the following values: 0%, 40%, 80%, 100%, 120%. RH 120% means that 20% of extra water is injected in liquid phase in the gas channel while the gas is already fully humidified. This latter case has not been considered in the present study. The dimensions of the GDL unit cell are indicated in the caption of Fig. 2.

First insights from MIPNM simulations

As a first step to study the impact of the anode operating conditions, i.e. RH_a, on the liquid water distribution in the cathode GDL, we have simply played with the partition co efficients β and γ of the MIPNM in order to mimic the change in RH_a. The fraction β of produced water flux going to the cathode side is a relevant parameter to mimic the impact of RH_a on the liquid water distribution at the cathode side. Indeed, it can be surmised that the fraction of produced water flux going to ward the cathode side increases as RH_a is increased. Further more, the fraction γ of the produced heat flux going toward the cathode side can be seen as a second relevant parameter to take into account the impact of RH_a. As can be seen from Fig. 1, there can be liquid water nowhere, or only on the cathode side, or on both the anode and the cathode sides depending on the values of RH_a and RH_c. This change in liquid water distribution in the whole anode cathode assembly might reflect some change in the balance between the fraction of the heat flux $\gamma\Phi$tot going toward the cathode side and the complementary fraction (1 $\gamma)\Phi$tot going toward the anode side. The density of liquid injection points α can also impact the liquid water distribution on the cathode side. However, it has not been tried to play with this parameter in the present study. It has been shown in Ref. [30] that α 20% led to liquid water distributions in the cathode consistent with in situ

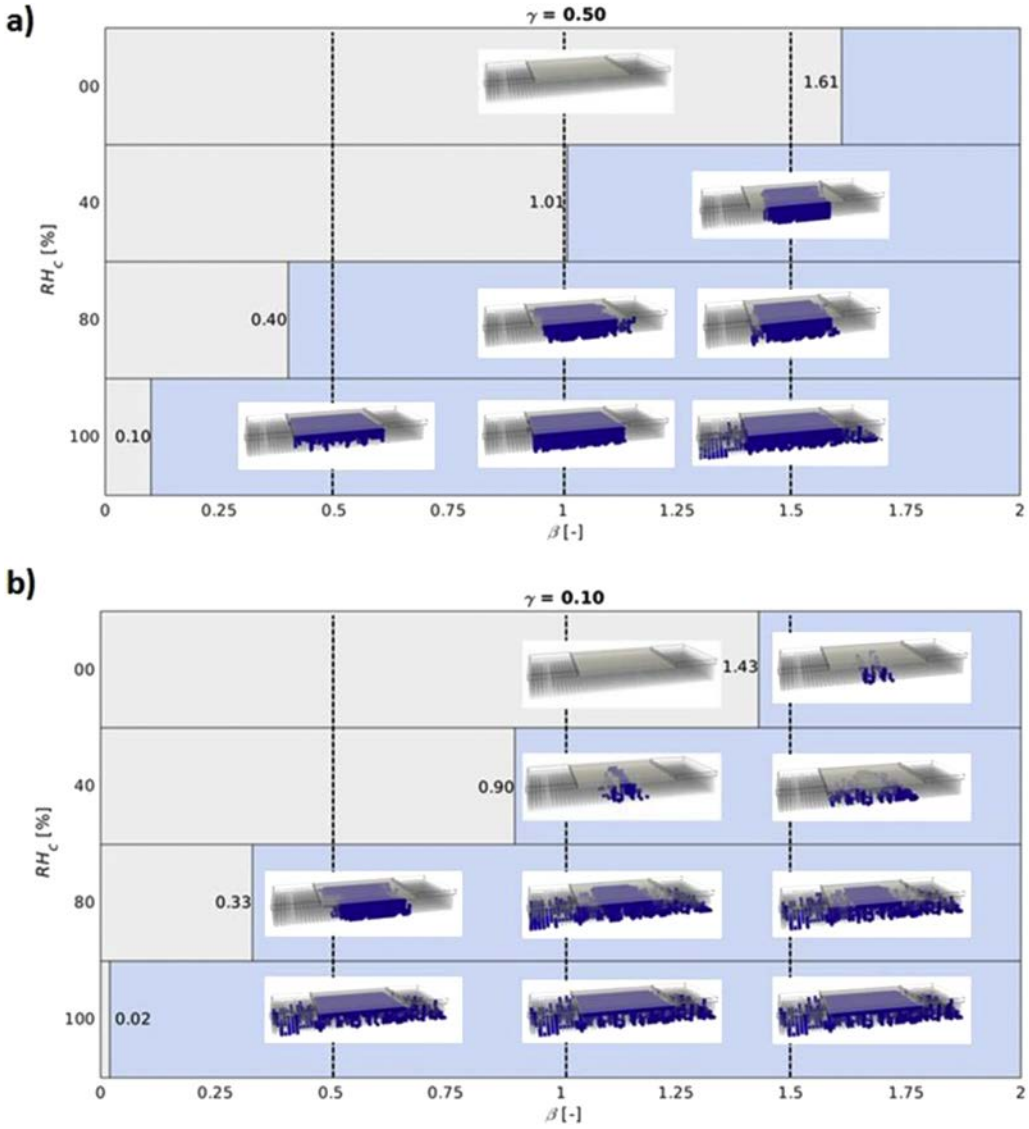

Fig. 3 – Dry-wet regime diagram obtained for γ 0.50 (a) and γ 0.10 (b). In the grey region the cathode GDL remains dry while in the blue region the cathode GDL contains liquid water. Some computed liquid water distributions are shown (the central region is the region below the rib). The figures at the vertical lines between the blue and grey regions are the transition value β_{dw} corresponding to the transition between the dry regime in which the cathode GDL remains dry and the wet regime in which the cathode GDL contains liquid water. (For interpretation of the references to colour in this figure legend, the reader is referred to the Web version of this article.)

experimental observations. For this reason, the value of α is not varied in the present study and kept equal to 20%.

For each considered value of RH_c, simulations have been performed with different values of the partition coefficients β and γ. Each simulation is thus characterized by its inputs and model parameters, namely RH_c, β, γ. β has been varied in the range [0.01, 2.0]. β 1 means that all the water produced by the electrochemical reaction goes toward the cathode side. $\beta > 1$ means that all the water produced by the reaction goes toward the cathode side and that some extra water is transferred from the anode to the cathode because of the greater RH_a compared to RH_c.

The following values of γ have been tested: 0.1, 0.2, 0.3, 0.4, 0.5, 0.6. γ 0.5 means that half of the produced heat flux goes toward the cathode side. Lower values of γ mimic the situa tions where the anode is cooler than the cathode for instance. Values of γ slightly greater than 0.5 mimic an asymmetry in the heat flux partition between the cathode side and the anode side.

The main objective here is to reproduce for each given value of RH_c the transition in the water distribution in the cathode GDL from the dry regime in which the GDL is totally dry, to the condensation regime in which liquid water is only present in the region below the rib, and finally to the mixed

Table 2 – Parameters of the 1D model with geometrical parameters in the 2nd column, water transfer parameters in the 3rd column and thermal transfer parameters in the 4th column; A. stands for anode and C. for cathode.

A. BP	δ_{ch}	600 μm			$k_{th,BP}$	0.85 W m $^{-1}$ K $^{-1}$	
A. GDL	δ_{GDL}	200 μm	$D^*_{GDL,a}$	7.43×10^{-6} m^2 s $^{-1}$	$k_{th,dryGDL}$	0.85 W m $^{-1}$ K $^{-1}$	
A. CL	δ_{CL}	10 μm	$D^*_{CL,a}$	4.5×10^{-7} m^2 s $^{-1}$ [55]	$k_{th,CL}$	0.27 W m $^{-1}$ K $^{-1}$	[56]
MEM.	δ_m	18 μm	D_m	2.5×10^{-10} m^2 s $^{-1}$ [42]	$k_{th,m}$	0.25 W m $^{-1}$ K $^{-1}$	[57]
			n_{drag}	2.5 [45]			
			ρ_m	1970 kg m^3 [46]			
			M_m	1.1 kg mol [46]			
C. CL	δ_{CL}	10 μm	$D^*_{CL,c}$	4.5×10^{-7} m^2 s $^{-1}$ [55]	$k_{th,CL}$	0.27 W m $^{-1}$ K $^{-1}$	[56]
C. GDL	δ_{GDL}	200 μm	$D^*_{GDL,c}$	2.05×10^{-6} m^2 s $^{-1}$	$k_{th,dryGDL}$	0.85 W m $^{-1}$ K $^{-1}$	
C. BP	δ_{ch}	600 μm			$k_{th,BP}$	0.85 W m $^{-1}$ K $^{-1}$	

regime characterized by the presence of liquid water both in the regions below the rib and below the channels.

Results

Fig. 3 shows the dry wet GDL regime diagram obtained for two values of the heat partition coefficient γ (γ 0.5 in Fig. 3a and γ 0.1 in Fig. 3b). For each value of RH_c, the transition value β_{dw} corresponding to the transition between the dry regime in which the cathode GDL remains dry and the wet regime in which the cathode GDL contains liquid water is indicated. Some liquid water distributions in the cathode GDL are also shown in the diagram for β 0.5, β 1 and β 1.5.

One can first notice that β_{dw} decreases as RH_c increases for a given value of γ. This means that the lower RH_c, the higher is the flow rate of water going on the cathode side necessary for the occurrence of liquid water in the cathode GDL. In particular, it is interesting to see that for low values of RH_c (see the cases $RH_c \leq 40\%$ for γ 0.5 in Fig. 3a), the MIPNM predicts that β_{dw} must be higher than 1.0 for the cathode GDL to be in the wet regime. In other words, the water flux going toward the cathode side must be greater than the water flux produced by the electrochemical reaction for liquid water to be present in the cathode GDL.

A second interesting result is that β_{dw} decreases when γ decreases for a given value of RH_c. This was somewhat expected since a reduced heat flux leads to lower temperature variations in the GDL, which consequently favours the water vapour condensation. For γ 0.1 and RH_c 100%, β_{dw} is quite small. This means that the presence of liquid water in the cathode GDL is certain, whatever the imposed relative humidity RH_a in the gas in the anode channels.

Also, the results shown in Fig. 3 illustrate the impact of heat transfer on the liquid water distribution. For the greater value of γ the liquid distribution is dominated by condensation effect as the results of greater temperature variations in the cathode GDL. As a result, liquid water is confined below the rib with liquid water in the regions below the channel only for the highest β. In contrast, for the lower value of γ, the temperature variation within the GDL is less, the condensation effect is less and there is comparatively more liquid water in the region of the GDL below the channels. Thus a mixed regime is observed for a sufficiently low value of γ.

In summary, these simulations lead to first insights consistent with the experimental observations recalled in Fig. 1. Firstly, it is possible to obtain a transition from the dry regime to the wet regime by varying the MIPNM partition coefficients (β, γ). Furthermore, for a given RH_c, it is possible to go from one liquid water scenario to another. For instance, for γ 0.50 and RH_c 100% (see Fig. 3a), the condensation scenario with liquid water only below the rib is obtained for β 0.5 while it is possible to reach the mixed regime for β 1.5. Also, it is possible to transit from the condensation scenario to the mixed scenario by reducing γ (see the case RH_c 100% and β 0.5 for γ 0.5 and γ 0.1).

These first results are encouraging as regards the ability of the MIPNM to take into account the anode operating conditions by means of the partition coefficients. However, one can wonder if the quite high values of β necessary for obtaining the occurrence of liquid water for RH_c 0% or also the low values of γ explored are really consistent, i.e. have a physical meaning or not. To get insights into this issue, a full anode cathode model enabling one to solve the heat and vapour transfers in the full anode cathode assembly has been developed. The model is presented in the next section.

Full anode-cathode assembly 1D model

The 1D model enables one the computation of the transfers in the different layers of the anode cathode assembly in the through plane direction. The thicknesses of the different layers are reported in Table 2 and the anode cathode assembly is sketched in Fig. 4. Note that the MPL is not taken into account in this model. The thicknesses in Table 2 correspond to the fuel cell stack used in Refs. [10] with Sigracet 24BC gas diffusion layers and a catalyst coated membrane of type Primea 5710 (Gore Ltd., USA).

Water transfer 1D model

The water transport is assumed to occur in vapour phase in the various porous layers under steady state conditions. Based on the results from Ref. [30], this assumption is consistent with the fuel cell operating conditions leading to the dry regime for which the cathode GDL remains dry and also for the wet condensation regime where the formation of liquid water in the cathode GDL is due to the vapour condensation only. This also means that the present model is not adapted to the conditions corresponding to the mixed

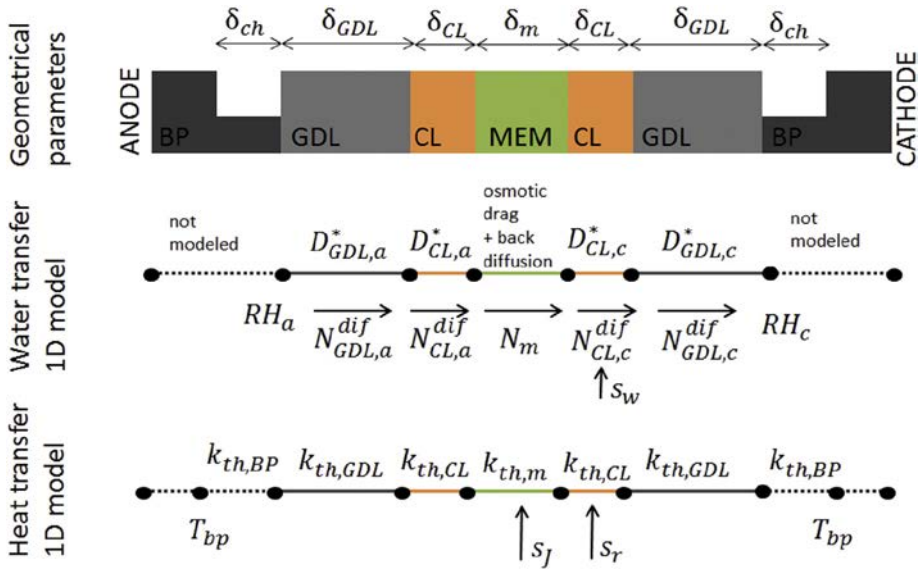

Fig. 4 – 1D model: geometrical parameters (top) and schematics of water transfer problem (middle) and heat transfer problem (bottom).

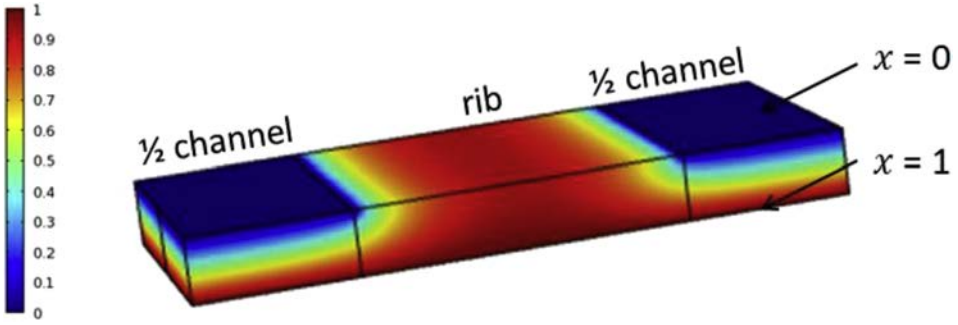

Fig. 5 – Water vapour molar fraction distribution in the cathode GDL unit cell obtained from continuum simulation with x 0 imposed at the GDL-channel interface and x 1 at the GDL – CL (MPL) interface.

regime [30]. The water transfer problem is sketched in Fig. 4. Depending on the considered layer, different phenomena are taken into account.

For the GDLs and the CLs, the water vapour is transferred by diffusion. The problem to be solved reads,

$$\nabla.\left(N_{i,j}^{dif}\right) \quad s_{i,j} \tag{3}$$

where $s_{i,j}$ is the local source term in the considered layer and $N_{i,j}^{dif}$ is the water vapour diffusive flux,

$$N_{i,j}^{dif} \quad D^{*}\frac{c\left(x_i \quad x_j\right)}{\delta} \tag{4}$$

where D^{*} is the effective diffusion coefficient, $c \quad \frac{P_{ref}}{RT_{bp}}$ is the mole concentration of the gas phase defined at the BP temperature T_{bp}, x_i is the water vapour molar fraction and δ is the layer thickness. For each layer, the effective diffusion coefficients D^{*} has been calculated from binary gas diffusion coefficient D at the given operating conditions (T_{bp}, P) considering the gas as a mixture of air and water vapour at the cathode and hydrogen and water vapour at the anode. $D^{*} \quad \tau D$ where τ can be considered as a tortuosity coefficient. However, for the CLs, the values D_{CL}^{*} are directly provided by experimental measurements (see Table 2). For the GDL, τ takes into account two effects: the GDL microstructure impact and the impact due to the rib/channel geometry. Indeed, the latter impacts the global diffusion of water vapour since the path ways to reach the catalyst layer located below the rib from the channel are longer than the pathways to reach the catalyst layer right below the channel. This phenomenon is illustrated in Fig. 5 with the computation of the water vapour molar fraction in the GDL unit cell when $x \quad 0$ is imposed at the GDL channel interface and $x \quad 1$ at the GDL CL (MPL) interface. In the present study, τ has been set to 0.12 in the GDLs. This value has been obtained from both pore network simulations and continuum simulations (using the commercial code COMSOL Multiphysics) considering a dry GDL unit cell. The value of the effective diffusion coefficient will not be changed

in the presence of liquid water in the cathode GDL for simplicity. This assumption will be discussed later.

Various models describing the water transfer in the membrane are reviewed in Ref. [58] where it is advised to use a diffusive model when the membrane is not fully hydrated. The model developed by Springer et al. [42] is one of the first models considering this option. In this model, the water flux in the membrane is expressed as,

$$N_m \quad N_{drag} + N_{bdif} \tag{5}$$

where N_{drag} is the electro osmotic drag flux and N_{bdif} is the back diffusion flux.

The electro osmotic drag flux is a function of the water content in the membrane [42]. As in Ref. [59], the latter is computed as the mean value of the water contents $\lambda_{H2O,a}$ and $\lambda_{H2O,c}$ where $\lambda_{H2O,a}$ and $\lambda_{H2O,c}$ are the water contents at the anode CL membrane interface and at the cathode CL membrane interface respectively,

$$\lambda_{H2O,m} \quad \frac{\lambda_{H2O,a} + \lambda_{H2O,c}}{2} \tag{6}$$

The electro osmotic drag flux N_{drag} is then expressed as,

$$N_{drag} \quad 2n_{drag}\frac{\lambda_{H2O,m}}{22}\frac{i}{2F} \tag{7}$$

where n_{drag} is the drag coefficient, i.e the number of molecules of water dragged per proton, and F is the Faraday's constant. $\frac{i}{2F}$ is the flux of water produced by the electrochemical reaction which is also the flux of H_2 in the electrochemical reaction. The factor 2 comes from the fact that the flux of proton $H+$ is twice the flux of H_2. The back diffusion flux is commonly expressed as [42–45,59],

$$N_{bdif} \quad D_m\frac{\rho_m}{M_m}\frac{\lambda_{H2O,c} \quad \lambda_{H2O,a}}{\delta_m} \tag{8}$$

where D_m is the diffusion coefficient of water in the membrane, ρ_m is the dry membrane density, M_m is the membrane molecular weight and δ_m is the thickness of the membrane. The diffusion coefficient of water in the membrane is actually water content dependent [42]. However, it has been chosen to set D_m as constant for simplicity in the present model.

The water content is calculated at the CL membrane interface at the anode and cathode sides using the sorption relation experimentally obtained by Hinatsu et al. at 80 °C [60],

$$\lambda_{H2O,i} \quad 0.3 + 10.8\left(\frac{x_i P_{ref}}{P_{sat}(T)}\right) \quad 16\left(\frac{x_i P_{ref}}{P_{sat}(T)}\right)^2 + 14.1\left(\frac{x_i P_{ref}}{P_{sat}(T)}\right)^3 \tag{9}$$

where x_i is the water vapour molar fraction, P_{sat} is the saturation pressure, P_{ref} is the gas phase pressure (P_{ref} P in our model) and T is the local temperature at the interfaces computed with the heat transfer 1D model.

In the cathode CL, the water produced by the electrochemical reaction is modelled as a source term:

$$s_w \quad \frac{i}{2F} \tag{10}$$

The inputs of the 1D model are the current density i and the values of the relative humidity RH_a and RH_c in the gas at the anode and the cathode, respectively (see Fig. 4). The values of the parameters for the various layers are specified in Table 2.

The water transfer problem leads to a non linear system of equations due to the fact that the membrane water flux N_m is a function of the water contents $\lambda_{H2O,a}$ and $\lambda_{H2O,c}$ at the interface between the CLs and the membrane (see Eqs. (5), (7) and (8)). $\lambda_{H2O,a}$ and $\lambda_{H2O,c}$ are a non linear function of the water vapour molar fraction x (see Eq. (9)). The algorithm developed to solve the water transfer problem can be summarized as follows:

- Pairs of ($RH_{m,a}$, $RH_{m,c}$) are chosen. $RH_{m,a}$ ($RH_{m,c}$ respectively) is the values of the relative humidity at the anode (cathode respectively) CL membrane interface. RH_m is varied in the range [0, 1]. The range is split into 10,000 values.
- Eq. (9) is used to determine $\lambda_{H2O,a}$ and $\lambda_{H2O,c}$
- Eqs. (5), (7) and (8) are used to determine N_m.
- The water transfer problem, i.e. Eqs. (3) and (4), is solved in the anode GDL and CL. The boundary conditions are RH_a and $RH_{m,a}$. This yields $N_{GDL,a}$ $N_{CL,a}$.
- The water transfer problem, i.e. Eqs. (3) and (4), is solved in the cathode GDL and CL. The boundary conditions are RH_c and $RH_{m,c}$ and a source term, Eq. (10), is taken into account in the cathode CL. This yields $N_{CL,c}$ which is the water flux at the cathode CL membrane interface.

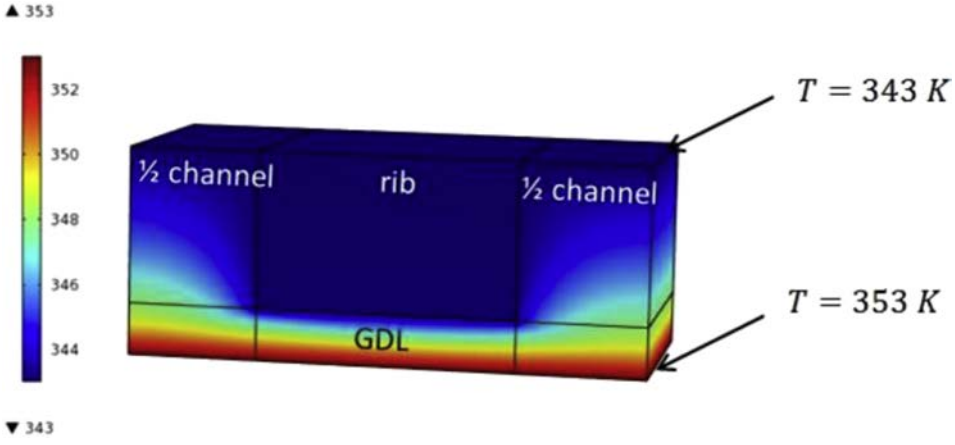

Fig. 6 – Temperature distribution in the BP and the GDL for a temperature variation of 10 °C.

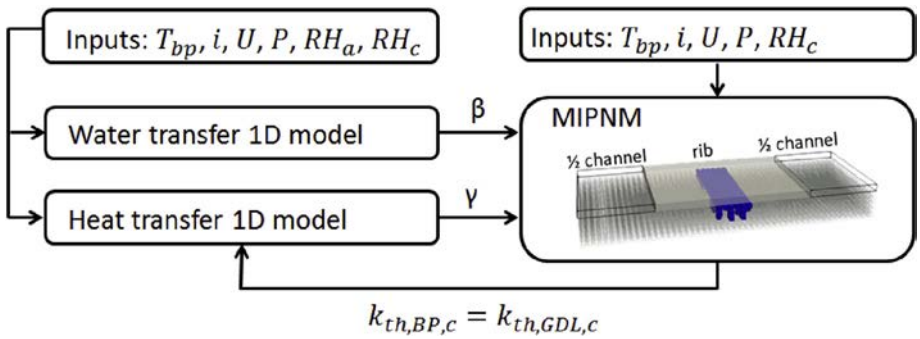

Fig. 7 – Schematic of the coupling between the full anode-cathode assembly 1D model and the cathode GDL MIPNM.

- The solution must fulfil the condition $N_m \quad N_{CL,a} \quad N_{CL,c}$. For each pair of ($RH_{m,a}$, $RH_{m,c}$) the relative error is assessed:

$$\xi \quad \frac{N_m \quad N_{CL,a|} + |N_m \quad N_{CL,c}}{|N_m|} \tag{11}$$

- The ($RH_{m,a}$, $RH_{m,c}$) pair minimizing the relative error is chosen if the relative error is small enough, i.e. $\xi < 10^{-2}$. When no pair is found fulfilling the condition $N_m \quad N_{CL,a} \quad N_{CL,c}$, this means that no solution can be found under the assumption of water transferred in vapour phase only.

Heat transfer 1D model

The heat transfer problem is solved over the whole anode cathode assembly as sketched in Fig. 4. The heat is transferred through the layers by conduction,

$$\nabla.(k_{th}\nabla T) \quad s \tag{12}$$

where k_{th} is the thermal conductivity in the through plane direction of each layer and s is the source term. It must not be confused with the overall liquid water saturation S in the cathode GDL.

The used values for the thermal conductivities in each layer are reported in Table 2. One assumption made for the computation of the GDL thermal conductivity needs explanation. The temperature distribution in the BP and the GDL is plotted in Fig. 6 when a thermal difference of 10 °C is imposed between the bipolar plate and the CL (MPL) – GDL interface. As it can be seen, the temperature distribution is significantly impacted by the rib channel geometry of the BP. This is due to the much lower thermal conductivity of the gas in the channel compared to the rib thermal conductivity. In order to take into account this 2D effect in the 1D model, the 1D thermal conductivity of the BP GDL assembly is imposed in both the GDL and the BP regions, i.e. $k_{th,BP} \quad k_{th,GDL}$. This global thermal conductivity is computed by solving the 3D heat transfer problem in the GDL unit cell and the adjacent BP using the MIPNM. This is explained further below (see Eq. (17)). This permits to take into account the rib/channel effect in the 1D transfer model. Furthermore, this thermal conductivity is dependent on the liquid water distribution of the GDL. The value of $k_{th,BP}$ and $k_{th,GDL}$ reported in Table 2 is the one for a dry GDL. The presence of liquid water in the GDL increases the thermal conductivity (see Eq. (17) below).

Two heat source terms are considered. In the cathode CL, the exothermic electrochemical reaction releases heat,

$$s_r \quad h_r \frac{i}{2F} \tag{13}$$

Joule heating is considered in the membrane only. This assumption can be made because of the different orders of magnitude between the electrical conductivity of the GDL or CL and that of the membrane [33]. Joule heating is expressed as:

$$s_J \quad Ui \tag{14}$$

As boundary conditions for the heat transfer problem, the BP temperature T_{bp} is imposed. This temperature is specified at the interface between the channel and the BP as depicted in Fig. 4.

Coupling the 1D model with the MIPNM

A schematic of the coupling between the full anode cathode assembly 1D model and the cathode GDL MIPNM is depicted in Fig. 7. The inputs of the coupled model are: the BP temperature T_{bp}, the current density i, the voltage U, the pressure P and the relative humidities RH_a and RH_c in the gas at the anode and the cathode, respectively. The value of the voltage is specified as in Ref. [10]. In what follows, unless otherwise mentioned, $U \quad 0.54$ V. The coupling algorithm between the 1D model and the MIPNM can be summarized as follows.

Step 0 Initially, the cathode and anode GDLs are dry.

Step 0 bis The thermal conductivities kth, BP kth, GDL at the cathode side are the ones for a dry GDL (Table 2).

Step 1 The heat transfer 1D model is solved. The temperature field along the full anode cathode assembly is computed. From this temperature field, the fraction γ of the produced heat flux going toward the cathode side is determined,

$$\gamma \quad \left(k_{th,GDL,c}\frac{T_{CL\ GDL,c} \quad T_{BP\ GDL,c}}{\delta_{GDL}}\right)\frac{1}{s_r + s_J} \tag{15}$$

where $T_{CL\ GDL,c}$ is the temperature at the cathode CL GDL interface, $T_{BP\ GDL,c}$ is the temperature at the cathode BP GDL interface.

Step 2 The water transfer 1D model is solved. The water vapour molar fraction is computed (if the algorithm con verges). The fraction β of water flux going toward the cathode side is determined,

$$\beta \quad \left(D^{*}_{GDL,c}\frac{c(x_{CL\ \ GDL,c} \quad x_{BP\ \ GDL,c})}{\delta_{GDL}}\right)\frac{1}{s_w} \tag{16}$$

where $x_{CL\ \ GDL,c}$ is the water vapour molar fraction at the cathode CL GDL interface and $x_{BP\ \ GDL,c}$ is the water vapour molar fraction at the cathode BP GDL interface.

Step 3 The water formation and transport in the cathode GDL is computed with the MIPNM. The value of γ determined in step (1) and β determined in step (2) are used as input pa rameters for the MIPNM simulation.

Step 4 The thermal conductivities $k_{th,BP}$ $k_{th,GDL}$ at the cathode side are modified when the cathode GDL is not dry anymore (the anode GDL is always considered dry):

$$k_{th,BP} \quad k_{th,GDL} \quad \gamma(s_r + s_J)\frac{\delta_{GDL} + \delta_{BP}}{T_{mean,CL\ \ GDL} \quad T_{bp}} \tag{17}$$

where $T_{mean,CL\ \ GDL}$ is the mean value of the temperature at the cathode CL GDL interface computed with the MIPNM for the wet GDL.

Step 5 Steps (1) to (4) are repeated until convergence of γ and β. The convergence is assessed at each step using Eq. (18),

$$\varepsilon \quad \beta^{n} \quad \beta^{n\ 1} + \gamma^{n} \quad \gamma^{n\ 1} \tag{18}$$

After convergence, the 1D model provides the final values of γ and β and the MIPNM provides the liquid water distribu tion in the cathode GDL.

Note that we are primarily interested in regimes where the GDL is not highly flooded because of the assumption of no liquid water in the CL in the 1D model. Under these circum stances, the effective diffusion coefficient of the GDL/BP as sembly varies little with the liquid saturation in the GDL because the saturation in the regions below the channels in the GDL is low. As a result, the impact of the change in the GDL saturation as computed by the MIPNM on the vapour diffusive transport in the GDL is neglected in the 1D model. Thus the main impact of the coupling is through the effective thermal

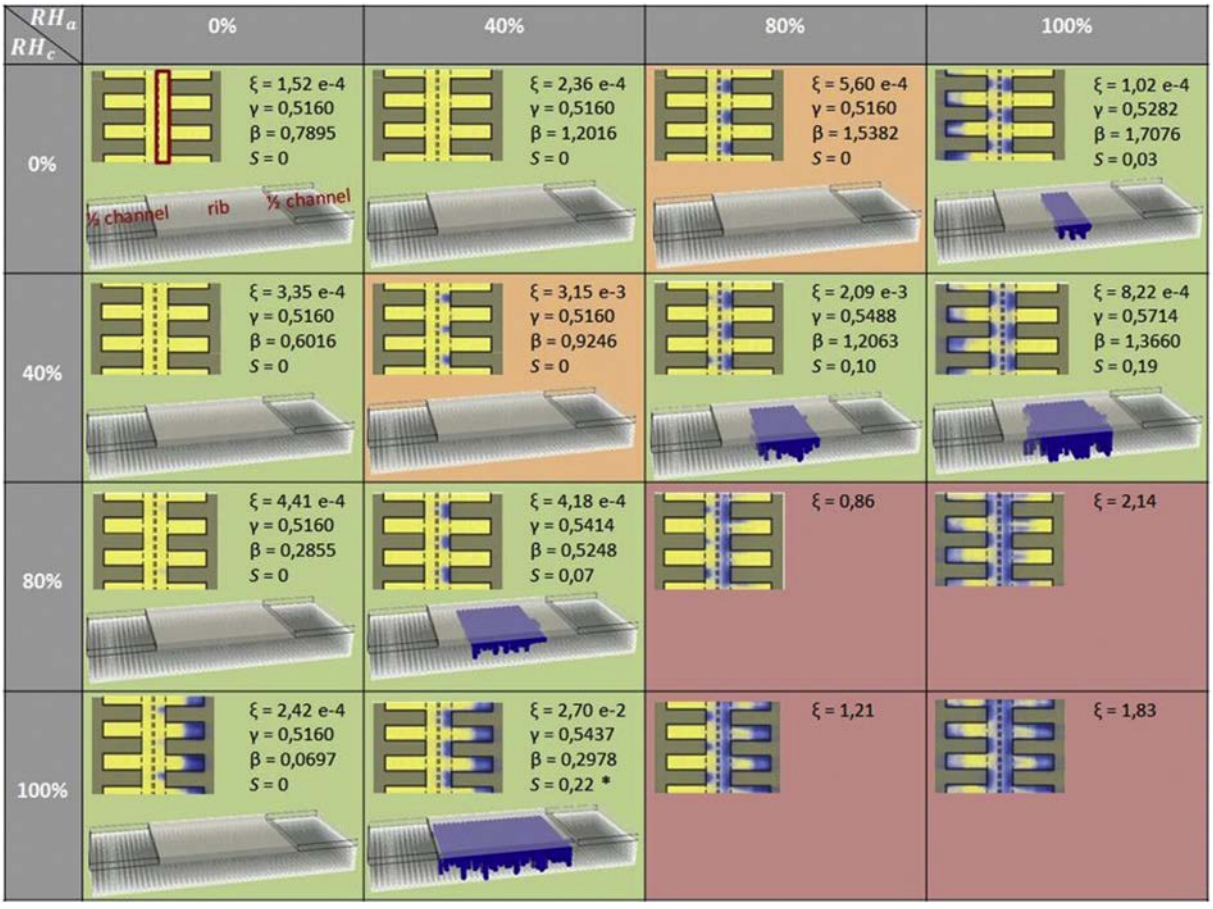

Fig. 8 – Comparison between the results obtained from the coupled model and experimental observations from Ref. [10]. For each case, the liquid water (in blue) distribution (blue, brown, yellow panels for the experimental distributions, 3D renderings for the ones computed with the coupled model) is shown and the values of γ, β, ξ (Eq. (11)), and S are given (Republished with permission of Electrochemical Society Inc., from [Local Characterization of PEFCs by Differential Cells: SystematicVariations of Current and Asymmetric Relative Humidity, P. Oberholzer & P. Boillat, Journal of the Electrochemical Society, 161 (1), 2014]; permission conveyed through Copyright Clearance Center, Inc.). (For interpretation of the references to colour in this figure legend, the reader is referred to the Web version of this article.)

conductivity of the GDL/BP assembly. The latter is updated according to Eq. (17) using the temperature field computed with the MIPNM. This modification in the 1D model leads to new values of β and γ and so on until convergence.

Coupled model results

The experimental conditions from Ref. [10] have been used to perform simulations with the coupled model. The operating conditions, as reported in Table 1, are: T_{bp} 70 °C, i 1 A cm ^{2} and P 2 bar. All the pairs of (RH_a, RH_c) obtained by combining the four values: 0%, 40%, 80%, 100%, have been simulated.

The objective is to validate the coupled model as regards its ability to take into account the impact of the anode operating conditions on the liquid water distribution in the cathode GDL.

Fig. 8 presents the comparison between the experimental data from Ref. [10] and the results from the coupled model obtained for all the considered pairs (RH_a, RH_c). The liquid water distribution computed by the coupled model for each converged simulation is shown. The final value of heat flux partition coefficient γ and water flux partition coefficient β, the overall liquid water saturation S in the cathode GDL and the relative error ξ, Eq. (11), obtained by solving the water transfer 1D problem are given in Fig. 8. The red box on the experimental liquid water distribution for the pair (RH_a 0%, RH_c 0%) indicates the cathode GDL. The background colour code in Fig. 8 is commented further below.

Comparisons with experiments from Ref. [10]

The convergence in solving the water transfer 1D problem is first commented (see the values of ξ indicated in Fig. 8). For the highest values of RH_a and RH_c, i.e. when both RH_a and RH_c are equal to 80% or 100%, a solution to the water transfer 1D problem cannot be found. These cases are indicated with a red background in Fig. 8. For these cases, the minimal relative error ξ is too high, i.e. greater than 0.01, for considering that the convergence has been reached. This means that no solution with relative humidities at the membrane interfaces lower than 100% can be found. This non convergence is therefore interpreted as an indication that all the produced water cannot be transferred in vapour phase for these cases. This is consistent with the experimental visualizations in Ref. [10] showing that both the anode and the cathode GDLs contain liquid water for these operating conditions. In other words, this non convergence is considered as a result, an indication that liquid water should be present elsewhere than simply in the cathode GDL. One can also notice that ξ is quite high for the case (RH_a 40%, RH_c 100%), this is due to the fact that the relative humidity at the membrane interfaces is close to 1.

For all the cases shown with a green background in Fig. 8, the coupled model predicts dry or wet regime in agreement with the experimental data. However, for a given value of RH_c the coupled model does not always separate the dry and wet regimes accurately. For RH_c 0% and RH_c 40% for instance, a disagreement in terms of dry wet regime between the numerical results from the coupled model and the experimental data is obtained for the intermediate values of RH_a 80% and 40% respectively. The background of these cases is in orange in Fig. 8. For these cases, it has been tried to modify the value of the voltage U. The simulation has been run with the exact value of U reported in Ref. [10]. One could hope that the impact of U on the heat transfer problem might resolve the disagreement observed between the numerical results and the experimental data. However, this has not been successful. Nevertheless, this has shown that β increases with increasing U.

Finally, the convergence of the coupled model is operating conditions dependent. For all the conditions leading to the dry regime, there is of course no convergence problem. Also, for most wet regime conditions with the green background in Fig. 8, the convergence of the iterative algorithm is straight forward. Only a few iterative steps are necessary to converge. However, the convergence is less simple for some borderline cases. For instance, for RH_a 40% and RH_c 100%, the iterative algorithm has led to a solution oscillating between two results with the number of iterations. For instance, the overall saturation S oscillated between 0.12 and 0.22, the relative variations of other parameters being much less (for instance β oscillated between 0.27 and 0.31). This is the only wet case for which the convergence of the water transport 1D problem has been problematic. The results reported in Fig. 8 correspond to the ones for which ε, i.e. the difference between two successive iterations as computed using Eq. (18), was the lowest. Perhaps here some relaxation strategy between two successive iterations might eliminate the oscillations. This has not been attempted since the convergence was quite good for the other conditions (green backgrounds in Fig. 8).

As already explained, it has been chosen to keep the tortuosity coefficient τ constant. After each iterative step, the value of τ has been determined to see the impact of the presence of liquid water, if any, in the cathode GDL. It has been found that the value of τ in the presence of water remains in the range [0.11, 0.13], thus close to its fixed value 0.12. This validates our assumption on τ. However, one should keep in mind that only pure condensation patterns are obtained in these simulations. The impact of the liquid distribution on τ can be expected to be greater in the mixed regime [61].

On the partition coefficients

For all the conditions (RH_a,RH_c) leading to the dry regime the computed value of γ is the same as the cathode GDL remains dry and therefore the thermal conductivity of the cathode GDL is the same for all these cases. It can be noticed that the heat transfer 1D model predicts that γ 0.516, indicating a slight asymmetry consistently with the slightly off center position of the cathode catalyst layer where the heat is produced.

As can be seen from Fig. 8 the water partition coefficient β increases with increasing RH_a for a given value of RH_c (if one discards the case (RH_a 40%, RH_c 100%) for which, as discussed above, the convergence has been problematic). This result is logical. More water goes to the cathode side when the relative humidity at the anode side increases. Reversely, β decreases with an increasing RH_c for a given value of RH_a. This result could also be expected from the water mass balance. Furthermore, it is interesting to notice that β can be higher than 1 which means that the flux of water going toward the

cathode side is greater than the flux of water produced by the reaction (see the case RH_c 0% and RH_a 40% in Fig. 8).

The presence of liquid water in the cathode GDL impacts the heat transfer. First, the equivalent thermal conductivity of the cathode GDL increases when liquid water is present. Secondly, the fraction γ of generated heat going to the cathode side increases when liquid water is present. For instance, the model predicts that 57.14% of the heat is going to the cathode side for (RH_a 100%, RH_c 40%), which is higher than for the dry regime (γ 51.60%). It has been computed that γ would reach 70% if the cathode GDL is totally flooded (S 1). Thus the heat transfer tends to be more asymmetric as the liquid water content increases in the cathode GDL.

Conditions leading to the wet regime

The following five conditions lead to a wet regime associated with a converged solution of the model in our simulations: (RH_a 100%, RH_c 0%), (RH_a 80%, RH_c 40%), (RH_a 100%, RH_c 40%), (RH_a 40%, RH_c 80%) and (RH_a 40%, RH_c 100%). For all these cases, the coupled model predicts the presence of liquid water in the cathode GDL region only below the central rib, somewhat consistently with the fact that the 1D model does not converge when the conditions are such some water should enter the GDL directly in liquid form. This liquid water under the rib is formed by condensation of water vapour in that region which is the coldest region of the cathode GDL unit cell. As can be seen from Fig. 8, the overall liquid water saturation S is highly operating conditions dependent. S is considerably smaller for (RH_a 100%, RH_c 40%) than for (RH_a 40%, RH_c 100%). Only for (RH_a 100%, RH_c 40%), the liquid water saturation obtained with the coupled model seems in quantitative agreement with the experimental measurements in Ref. [10]. For the other cases, the water saturation in the cathode GDL predicted by the coupled model seems lower than the experimental value.

PEMFC dry wet regime cathode diagram with impact of anode humidity

The cathode GDL operating regime 3D diagrams obtained with the MIPNM considering the cathode side only have been pre sented in Ref. [30]. In other words, the impact of the operating conditions at the anode was neglected in Ref. [30]. So as to generalize the results from Ref. [30], the diagram has been computed considering the impact of the relative humidity RH_a at the anode by using the full anode cathode coupled model. The same range of operating conditions as in Ref. [30] has been considered. The temperature T_{bp} was varied and could take the following values: 30 °C, 40 °C, 50 °C, 60 °C, 70 °C, 80 °C, 90 °C. The current density i was varied considering the values: 0.25 A cm ^{2}, 0.5 A cm ^{2}, 0.75 A cm ^{2}, 1 A cm ^{2}, 1.25 A cm ^{2}, 1.5 A cm ^{2} whereas the relative humidity at the cathode RH_c was varied considering the values: 0%, 20%, 40%, 60%, 80%, 100%. The new operating condition considered with the full anode cathode 1D model is the relative humidity RH_a in the gas at the anode side. RH_a was varied considering the values: 0%, 20%, 40%, 60%, 80%, 100%. To perform the simulations, the voltage is specified from the same polarization curve as the

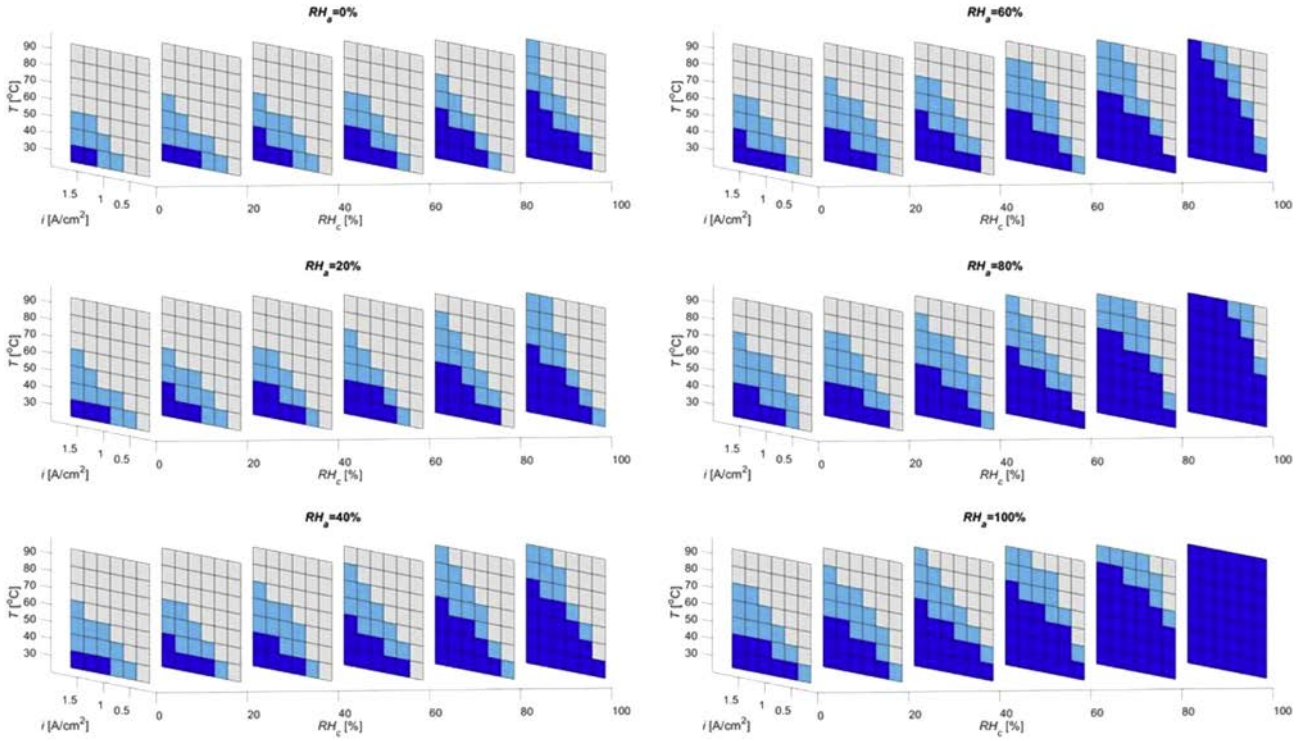

Fig. 9 – Dry-wet regime diagrams obtained with the full anode-cathode assembly 1D model. Each diagram corresponds to a different value of RH_a. The blue boxes represent the cases for which it can be concluded that liquid water is present in the cathode GDL. The grey boxes correspond to a regime where the cathode GDL is free from liquid water. (For interpretation of the references to colour in this figure legend, the reader is referred to the Web version of this article.)

one used in Ref. [30]. The pressure P was set to 1 bar as in Ref. [30].

In order to obtain the 3D regime diagram for each value of RH_a, it would have been necessary to simulate all the condi tions. This corresponds to 6 × 6 x 6 × 7 1512 simulations with the coupled model, which represents quite a lot of simulations. It is possible to construct the dry wet diagram with the coupled model without computing all these cases. It has been pointed out previously that the water transfer 1D model does not converge for some conditions (RH_a, RH_c), typically under highly humidified conditions. This is inter preted as an indication that all the produced water cannot be transferred in vapour phase only. Therefore, we can be sure that the anode cathode assembly will contain liquid water for such conditions. Also, it is fast to predict with the MIPNM whether the cathode GDL remains dry or not. This simply requires computing the initial relative humidity field in the cathode GDL and checking the local values (i.e. at the nodes of the pore network) of the relative humidity. If the local relative humidity is everywhere less than 1, the conditions corre spond to a dry regime. Otherwise, the conditions correspond to a wet regime. This computation has been performed for all the cases. It enables us to construct a dry wet regime diagram for each considered value of RH_a. The dry wet regime dia grams so obtained are shown in Fig. 9 for each considered value of RH_a. These diagrams differentiate the operating conditions (T_{bp}, i, RH_c) leading to the dry regime (grey boxes in Fig. 9) from the operating conditions leading to the wet regime (blue boxes in Fig. 9). Two different criteria leads to the identification of the wet regime: either the 1D water transfer model has not been able to converge (cases shown in dark blue in Fig. 9), or the 1D water transfer model converges at the first step of iteration but the computation of the initial dis tribution of RH in the cathode GDL using the MIPNM for the first step of iteration of the coupled model reveals that the cathode GDL will contain liquid water (cases shown in light blue in Fig. 9).

These new diagrams illustrate the impact of the relative humidity at the anode, namely RH_a. The higher is RH_a, the more likely the presence of liquid water in the fuel cell. In particular, it can be seen that whatever the temperature or the current density, there will always be liquid water for RH_a 100% and RH_c 100%. Overall, it can be concluded that the wet regime will be met for higher temperatures and or lower current densities when RH_a increases.

Conclusions

Numerical simulations have been developed for studying the impact of the humidity conditions on the anode side on the water distribution in the GDL on the cathode side. First, it has been shown that this impact could be taken into account with the pore network model presented in Ref. [30], namely the MIPNM, by playing with the parameters controlling the heat and water flux partition: the fraction γ of the heat flux going toward the cathode side and the fraction β of the water flux going toward the cathode side. A significant improve ment has then been to couple the MIPNM with a full anode cathode assembly 1D model. In this model, γ and β are not input parameters anymore but outcomes of the simulation. In this coupled model, the MIPNM is used to compute the water distribution in the cathode GDL whereas the 1D model is used for computing the heat and water transfers in the various components of the anode cathode assembly. It is worth mentioning that the MIPNM results do have an impact on the 1D model since the parameters on the 1D model, especially the cathode GDL thermal conductivity, is impacted by the liquid water presence in the GDL. On the whole, this model leads to quite consistent results with the experimental data reported in Ref. [10]. Since only water transfer in vapour form is considered in the various porous components of the anode cathode assembly (except for the cathode GDL where the liquid water formation by conden sation is computed using the MIPNM), the model does not converge for the highly humidified conditions. This non convergence is actually considered as the signature of a mixed wet regime where liquid water is present elsewhere than in the cathode GDL.

The coupled model has been used to compute diagrams delineating the operating conditions for which the cathode GDL is dry and the ones leading to a wet cathode GDL. These diagrams generalize the diagram reported in a previous pub lication by incorporating the impact of the anode humidity condition. These diagrams well illustrates that the conditions at the anode are a lever for the water management. In other words, playing with the conditions at the anode allows con trolling, at least in part, the liquid water on the cathode side and thus the gas access to the cathode CL.

The simulations well illustrate that considering the cath ode side only is too restrictive. The simulation of the water formation in the cathode GDL requires modelling the impact of the anode conditions.

Regarding the coupled model itself, improvements are desirable. A first improvement could be to explicitly take into account the MPL in the 1D model since the MPL have an impact on the heat transfer [51]. A challenge is to extend the model to situations where liquid water is present in the cathode CL (and MPL) for example so as to be in a position to consider the so called mixed regime [30] where a fraction of the water flux enters the cathode GDL directly in liquid form. In this respect, it is not obvious that a 1D continuum approach in the CL would be sufficient due to the discrete nature of the liquid water injection points in the GDL in the mixed regime. Also, the experimental results in Ref. [10] indicate that liquid water can be present also in the anode GDL for sufficiently humidified conditions at the anode side. Coupling the 1D model with the MIPNM also on the anode side is an option to deal with the corresponding regimes.

Acknowledgements

This research was supported by the Project “PEMFC – SUDOE” – SOE1/P1/E0293 which is co financed by the European Regional Development Fund in the framework of the Interreg Sudoe programme.

REFERENCES

[1] Eller J, Rosén T, Marone F, Stampanoni M, Wokaun A, Büchi FN. Progress in in situ X ray tomographic microscopy of liquid water in gas diffusion layers of PEFC. J Electrochem Soc 2011;158:B963. https://doi.org/10.1149/1.3596556.

[2] Eller J, Roth J, Marone F, Stampanoni M, Büchi FN. Operando properties of gas diffusion layers: saturation and liquid permeability. J Electrochem Soc 2017;164:F115 26. https://doi.org/10.1149/2.0881702jes.

[3] Chevalier S, Lee J, Ge N, Yip R, Antonacci P, Tabuchi Y, Kotaka T, Bazylak A. In operando measurements of liquid water saturation distributions and effective diffusivities of polymer electrolyte membrane fuel cell gas diffusion layers. Electrochim Acta 2016;210:792 803. https://doi.org/10.1016/j.electacta.2016.05.180.

[4] Chevalier S, Ge N, Lee J, George MG, Liu H, Shrestha P, Muirhead D, Lavielle N, Hatton BD, Bazylak A. Novel electrospun gas diffusion layers for polymer electrolyte membrane fuel cells: Part II. In operando synchrotron imaging for microscale liquid water transport characterization. J Power Sources 2017;352:281 90. https://doi.org/10.1016/j.jpowsour.2017.01.114.

[5] Muirhead D, Banerjee R, Lee J, George MG, Ge N, Liu H, Chevalier S, Hinebaugh J, Han K, Bazylak A. Simultaneous characterization of oxygen transport resistance and spatially resolved liquid water saturation at high current density of polymer electrolyte membrane fuel cells with varied cathode relative humidity. Int J Hydrogen Energy 2017;42:29472 83. https://doi.org/10.1016/j.ijhydene.2017.10.031.

[6] Liu H, George MG, Ge N, Banerjee R, Chevalier S, Lee J, Shrestha P, Muirhead D, Hinebaugh J, Zeis R, Messerschmidt M, Scholta J, Bazylak A. Accelerated degradation of polymer electrolyte membrane fuel cell gas diffusion layers: performance degradation and steady state liquid water distributions with in operando synchrotron X ray radiography. ECS Trans 2016;75:289 300. https://doi.org/10.1149/07514.0289ecst.

[7] Banerjee R, Ge N, Lee J, George MG, Chevalier S, Liu H, Shrestha P, Muirhead D, Bazylak A. Transient liquid water distributions in polymer electrolyte membrane fuel cell gas diffusion layers observed through in operando synchrotron X ray radiography. J Electrochem Soc 2017;164:F154 62. https://doi.org/10.1149/2.0991702jes.

[8] Banerjee R, Chevalier S, Liu H, Lee J, Yip R, Han K, Hong BK, Bazylak A. A comparison of felt type and paper type gas diffusion layers for polymer electrolyte membrane fuel cell applications using X ray techniques. J Electrochem Energy Conv Storage 2018;15:11002. https://doi.org/10.1115/1.4037766.

[9] Lee J, Chevalier S, Banerjee R, Antonacci P, Ge N, Yip R, Kotaka T, Tabuchi Y, Bazylak A. Investigating the effects of gas diffusion layer substrate thickness on polymer electrolyte membrane fuel cell performance via synchrotron X ray radiography. Electrochim Acta 2017;236:161 70. https://doi.org/10.1016/j.electacta.2017.03.162.

[10] Oberholzer P, Boillat P. Local characterization of PEFCs by differential cells: systematic variations of current and asymmetric relative humidity. J Electrochem Soc 2013;161:F139 52. https://doi.org/10.1149/2.080401jes.

[11] LaManna JM, Chakraborty S, Gagliardo JJ, Mench MM. Isolation of transport mechanisms in PEFCs using high resolution neutron imaging. Int J Hydrogen Energy 2014;39:3387 96. https://doi.org/10.1016/j.ijhydene.2013.12.021.

[12] Forner Cuenca A, Biesdorf J, Manzi Orezzoli V, Gubler L, Schmidt TJ, Boillat P. Advanced water management in PEFCs: diffusion layers with patterned wettability III. Operando characterization with neutron imaging. J Electrochem Soc 2016;163:F1389 98. https://doi.org/10.1149/2.0891613jes.

[13] Weber AZ, Borup RL, Darling RM, Das PK, Dursch TJ, Gu W, Harvey D, Kusoglu A, Litster S, Mench MM, Mukundan R, Owejan JP, Pharoah JG, Secanell M, Zenyuk IV. A critical review of modeling transport phenomena in polymer electrolyte fuel cells. J Electrochem Soc 2014;161:F1254 99. https://doi.org/10.1149/2.0751412jes.

[14] Sinha PK, Wang CY. Pore network modeling of liquid water transport in gas diffusion layer of a polymer electrolyte fuel cell. Electrochim Acta 2007;52:7936 45. https://doi.org/10.1016/j.electacta.2007.06.061.

[15] Sinha PK, Mukherjee PP, Wang CY. Impact of GDL structure and wettability on water management in polymer electrolyte fuel cells. J Mater Chem 2007;17:3089. https://doi.org/10.1039/b703485g.

[16] Hinebaugh J, Fishman Z, Bazylak A. Unstructured pore network modeling with heterogeneous PEMFC GDL porosity distributions. J Electrochem Soc 2010;157:B1651. https://doi.org/10.1149/1.3486095.

[17] Fazeli M, Hinebaugh J, Bazylak A. Investigating inlet condition effects on PEMFC GDL liquid water transport through pore network modeling. J Electrochem Soc 2015;162:F661 8. https://doi.org/10.1149/2.0191507jes.

[18] Gostick JT. Random pore network modeling of fibrous PEMFC gas diffusion media using voronoi and delaunay tessellations. J Electrochem Soc 2013;160:F731 43. https://doi.org/10.1149/2.009308jes.

[19] Wu R, Zhu X, Liao Q, Wang H, Ding Y, Li J, Ye D. A pore network study on water distribution in bi layer gas diffusion media: effects of inlet boundary condition and micro porous layer properties. Int J Hydrogen Energy 2010;35:9134 43. https://doi.org/10.1016/j.ijhydene.2010.06.051.

[20] Wu R, Zhu X, Liao Q, Wang H, Ding Y, Li J, Ye D. A pore network study on the role of micro porous layer in control of liquid water distribution in gas diffusion layer. Int J Hydrogen Energy 2010;35:7588 93. https://doi.org/10.1016/j.ijhydene.2010.04.126.

[21] Ji Y, Luo G, Wang CY. Pore level liquid water transport through composite diffusion media of PEMFC. J Electrochem Soc 2010;157:B1753. https://doi.org/10.1149/1.3491359.

[22] Qin X, Zhu S, Li Z, Chen S. Dynamic mechanical characterizations and road performances of flame retardant asphalt mortars and concretes. J Wuhan Univ Technol Materials Sci Ed 2015;30:1036 42. https://doi.org/10.1007/s11595 015 1269 4.

[23] Lee KJ, Nam JH, Kim CJ. Pore network analysis of two phase water transport in gas diffusion layers of polymer electrolyte membrane fuel cells. Electrochim Acta 2009;54:1166 76. https://doi.org/10.1016/j.electacta.2008.08.068.

[24] Lee KJ, Kang JH, Nam JH, Kim CJ. Steady liquid water saturation distribution in hydrophobic gas diffusion layers with engineered pore paths: an invasion percolation pore network analysis. J Power Sources 2010;195:3508 12. https://doi.org/10.1016/j.jpowsour.2009.11.141.

[25] Lee KJ, Kang JH, Nam JH. Liquid water distribution in hydrophobic gas diffusion layers with interconnect rib geometry: an invasion percolation pore network analysis. Int J Hydrogen Energy 2014;39:6646 56. https://doi.org/10.1016/j.ijhydene.2014.01.206.

[26] Zhan N, Wu W, Wang S. Pore network modeling of liquid water and oxygen transport through the porosity graded bilayer gas diffusion layer of polymer electrolyte membrane fuel cells. Electrochim Acta 2019;306:264 76.

[27] Médici EF, Allen JS. Evaporation, two phase flow, and thermal transport in porous media with application to low temperature fuel cells. Int J Heat Mass Tran 2013;65:779 88. https://doi.org/10.1016/j.ijheatmasstransfer.2013.06.035.

[28] Straubhaar B, Pauchet J, Prat M. Water transport in gas diffusion layer of a polymer electrolyte fuel cell in the presence of a temperature gradient. Phase change effect. Int J Hydrogen Energy 2015;40:11668 75. https://doi.org/10.1016/j.ijhydene.2015.04.027.
[29] Straubhaar B, Pauchet J, Prat M. Pore network modelling of condensation in gas diffusion layers of proton exchange membrane fuel cells. Int J Heat Mass Tran 2016;102:891 901. https://doi.org/10.1016/j.ijheatmasstransfer.2016.06.078.
[30] Carrere P, Prat M. Liquid water in cathode gas diffusion layers of PEM fuel cells: identification of various pore filling regimes from pore network simulations. Int J Heat Mass Tran 2019;129:1043 56. https://doi.org/10.1016/j.ijheatmasstransfer.2018.10.004.
[31] Carrere P, Prat M. Corrigendum to "Liquid water in cathode gas diffusion layers of PEM fuel cells: identification of various pore filling regimes from pore network simulations." [Int. J. Heat Mass Transfer 129. Int J Heat Mass Tran 2019;137:1323 5. https://doi.org/10.1016/j.ijheatmasstransfer.2019.03.035 (2019) 1043 1056].
[32] Belgacem N, Prat M, Pauchet J. Coupled continuum and condensation evaporation pore network model of the cathode in polymer electrolyte fuel cell. Int J Hydrogen Energy 2017;42:8150 65. https://doi.org/10.1016/j.ijhydene.2017.01.184.
[33] Aghighi M, Gostick J. Pore network modeling of phase change in PEM fuel cell fibrous cathode. J Appl Electrochem 2017;47:1323 38. https://doi.org/10.1007/s10800 017 1126 6.
[34] Qin CZ, Hassanizadeh S, Van Oosterhout L. Pore network modeling of water and vapor transport in the micro porous layer and gas diffusion layer of a polymer electrolyte fuel cell. Computation 2016;4:21. https://doi.org/10.3390/computation4020021.
[35] Hao L, Cheng P. Lattice Boltzmann simulations of water transport in gas diffusion layer of a polymer electrolyte membrane fuel cell. J Power Sources 2010;195:3870 81. https://doi.org/10.1016/j.jpowsour.2009.11.125.
[36] Molaeimanesh GR, Akbari MH. Impact of PTFE distribution on the removal of liquid water from a PEMFC electrode by lattice Boltzmann method. Int J Hydrogen Energy 2014;39:8401 9.
[37] Chen W, Jiang F. Impact of PTFE content and distribution on liquid gas flow in PEMFC carbon paper gas distribution layer: 3D lattice Boltzmann simulations. Int J Hydrogen Energy 2016;41:8550 62. https://doi.org/10.1016/j.ijhydene.2016.02.159.
[38] Niu Z, Bao Z, Wu J, Wang Y, Jiao K. Two phase flow in the mixed wettability gas diffusion layer of proton exchange membrane fuel cells. Appl Energy 2018;232:443 50. https://doi.org/10.1016/j.apenergy.2018.09.209.
[39] Alink R, Gerteisen D. Modeling the liquid water transport in the gas diffusion layer for polymer electrolyte membrane fuel cells using a water path network. Energies 2013;6:4508 30. https://doi.org/10.3390/en6094508.
[40] Alink R, Gerteisen D. Coupling of a continuum fuel cell model with a discrete liquid water percolation model. Int J Hydrogen Energy 2014;39:8457 73. https://doi.org/10.1016/j.ijhydene.2014.03.192.
[41] García Salaberri PA, Gostick JT, Zenyuk IV, Hwang G, Vera M, Weber AZ. On the limitations of volume averaged descriptions of gas diffusion layers in the modeling of polymer electrolyte fuel cells. ECS Trans 2017;80:133 43. https://doi.org/10.1149/08008.0133ecst.
[42] Springer TE. Polymer electrolyte fuel cell model. J Electrochem Soc 1991;138:2334. https://doi.org/10.1149/1.2085971.
[43] Ramousse J, Deseure J, Lottin O, Didierjean S, Maillet D. Modelling of heat, mass and charge transfer in a PEMFC single cell. J Power Sources 2005;145:416 27. https://doi.org/10.1016/j.jpowsour.2005.01.067.
[44] Lottin O, Antoine B, Colinart T, Didierjean S, Maranzana G, Moyne C, Ramousse J. Modelling of the operation of polymer exchange membrane fuel cells in the presence of electrodes flooding. Int J Therm Sci 2009;48:133 45. https://doi.org/10.1016/j.ijthermalsci.2008.03.013.
[45] Thomas A, Maranzana G, Didierjean S, Dillet J, Lottin O. Thermal and water transfer in PEMFCs: investigating the role of the microporous layer. Int J Hydrogen Energy 2014;39:2649 58. https://doi.org/10.1016/j.ijhydene.2013.11.105.
[46] Siegel NP, Ellis MW, Nelson DJ, von Spakovsky MR. A two dimensional computational model of a PEMFC with liquid water transport. J Power Sources 2004;128:173 84. https://doi.org/10.1016/j.jpowsour.2003.09.072.
[47] El Hannach M, Pauchet J, Prat M. Pore network modeling: application to multiphase transport inside the cathode catalyst layer of proton exchange membrane fuel cell. Electrochim Acta 2011;56:10796 808.
[48] El Hannach M, Prat M, Pauchet J. Pore network model of the cathode catalyst layer of proton exchange membrane fuel cells: analysis of water management and electrical performance. Int J Hydrogen Energy 2011;37:18996 9006.
[49] Grunewald JB, Mistry AN, Verma A, Goswami N, Mukherjee PP, Fuller TF. Perspective mesoscale physics in the catalyst layer of proton exchange membrane fuel cells. J Electrochem Soc 2019;166(7):F3089 92.
[50] Litster S, McLean G. Pem fuel cell electrodes. J Power Sources 2004;130(1):61 76.
[51] Zhou J, Shukla S, Putz A, Secanell M. Analysis of the role of the microporous layer in improving polymer electrolyte fuel cell performance. Electrochim Acta 2018;268(1):366 82.
[52] Zenyuk IV, Medici E, Allen J, Weber AZ. Coupling continuum and pore network models for polymer electrolyte fuel cells. Int J Hydrogen Energy 2015;40:16831 45. https://doi.org/10.1016/j.ijhydene.2015.08.009.
[53] Medici EF, Zenyuk IV, Parkinson DY, Allen J, Weber AZ. Understanding water transport in polymer electrolyte fuel cells using coupled continuum and pore network models. Fuel Cell 2016;16(6):725 33.
[54] Aghighi M, Hoeh MA, Lehnert W, Merle G, Gostick J. Simulation of a full fuel cell membrane electrode assembly using pore network modeling. J Electrochem Soc 2016;163(5):F384 92.
[55] Zhao J, Shahgaldi S, Alaefour I, Yang S, Li X. Pore structure and effective diffusion coefficient of catalyzed electrodes in polymer electrolyte membrane fuel cells. Int J Hydrogen Energy 2018;43:3776 85. https://doi.org/10.1016/j.ijhydene.2018.01.019.
[56] Khandelwal M, Mench MM. Direct measurement of through plane thermal conductivity and contact resistance in fuel cell materials. J Power Sources 2006;161:1106 15. https://doi.org/10.1016/j.jpowsour.2006.06.092.
[57] Burheim O, Vie PJS, Pharoah JG, Kjelstrup S. Ex situ measurements of through plane thermal conductivities in a polymer electrolyte fuel cell. J Power Sources 2010;195:49 256. https://doi.org/10.1016/j.jpowsour.2009.06.077.
[58] Weber AZ, Newman J. Modeling transport in polymer electrolyte fuel cells. Chem Rev 2004;104:4679 726. https://doi.org/10.1021/cr020729l.
[59] Dujc J, Forner Cuenca A, Marmet P, Cochet M, Vetter R, Schumacher JO, Boillat P. Modeling the effects of using gas diffusion layers with patterned wettability for advanced water management in proton exchange membrane fuel cells.

J Electrochem Energy Conv Storage 2018;15:21001. https://doi.org/10.1115/1.4038626.
[60] Hinatsu JT, Mizuhata M, Takenaka H. Water uptake of perfluorosulfonic acid membranes from liquid water and water vapor. J Electrochem Soc 1994;141:1493 8. https://doi.org/10.1149/1.2054951.
[61] Carrère P, Prat M. Impact of non uniform wettability in the condensation and condensation liquid water intrusion regimes in the cathode gas diffusion layer of proton exchange membrane fuel cell. Int J Therm Sci 2019;145:106045. https://doi.org/10.1016/j.ijthermalsci.2019.106045.